

1
2 **Sea Surface Salinity Provides Subseasonal Predictability for Forecasts of**
3 **Opportunity of U.S. Summertime Precipitation**
4

5 **Marybeth C. Arcodia¹, Elizabeth A. Barnes¹, Paul J. Durack², Patrick W. Keys¹, Juliette**
6 **Rocha³**
7

8 ¹Department of Atmospheric Science, Colorado State University, Fort Collins, CO, USA.

9 ²Program for Climate Model Diagnosis and Intercomparison (PCMDI), Lawrence Livermore
10 National Laboratory, Livermore, CA, USA.

11 ³Department of Atmospheric Science, Texas A&M University, College Station, TX, USA.

12 Corresponding author: Marybeth C. Arcodia (marcodia@rams.colostate.edu)

13 **Key Points:**

- 14 • Sea surface salinity anomalies provide predictability for heavy summertime Midwest
15 precipitation events
16 • Subseasonal forecasts of opportunity for heavy precipitation are informed by positive
17 salinity anomalies in the Caribbean and Gulf of Mexico
18 • Regions of evaporation identified by neural networks provide a direct moisture source for
19 precipitation in the Midwest region
20

21 **Abstract**

22 As oceanic moisture evaporates, it leaves a signature on sea surface salinity. Roughly 10% of the
23 moisture that evaporates over the ocean is transported over land, allowing the salinity fields to be
24 a predictor of terrestrial precipitation. This research is among the first in published literature to
25 assess the role of sea surface salinity for improved predictions on low-skill summertime
26 subseasonal timescales for terrestrial precipitation predictions. Neural networks are trained with
27 the CESM2 Large Ensemble using North Atlantic salinity anomalies to quantify predictability of
28 U.S. Midwest summertime heavy rainfall events at 0 to 56-day leads. Using explainable artificial
29 intelligence, salinity anomalies in the Caribbean Sea and Gulf of Mexico are found to provide
30 skill for subseasonal forecasts of opportunity, e.g. confident and correct predictions. Further, a
31 moisture-tracking algorithm applied to reanalysis data demonstrates that the regions of
32 evaporation identified by neural networks directly provide moisture that precipitates in the
33 Midwest.

34 **Plain Language Summary**

35 Global water cycling plays a fundamental role in the climate system, directly impacting
36 terrestrial water availability. Roughly 10% of the moisture that evaporates over the ocean is
37 transported over land, eventually falling as precipitation. As moisture evaporates from the ocean,
38 the waters below become saltier, leaving an imprint on the sea surface salinity pattern. These
39 salinity signatures can potentially be used as a predictor of landfalling precipitation in the
40 coming weeks. This study uses neural networks to quantify the predictability of summertime
41 precipitation in the Midwest from 0 to 56 days in advance using salinity patterns in the North
42 Atlantic. High salinity in the Caribbean Sea and Gulf of Mexico is found to provide skill for
43 subseasonal forecasts of opportunity, e.g. confident and correct predictions at 21-day leads. A
44 moisture-tracking model traces the origin of water that falls as precipitation and confirms the
45 Caribbean Sea and Gulf of Mexico as direct moisture sources for Midwest precipitation.
46

47 **1 Introduction**

48 Global water cycling plays a fundamental role in the climate system, directly impacting
49 terrestrial water availability. The hydrological cycle consists of moisture evaporation in one
50 location which falls as precipitation in another location via a balance of atmospheric, oceanic,
51 and terrestrial water transport (Adler et al., 2003; Gimeno et al., 2010). The majority of moisture
52 (~90%) that evaporates over the ocean rains out over the ocean (Trenberth et al., 2007).
53 However, the remaining 10% of the moisture evaporated is transported over land, eventually
54 falling as terrestrial precipitation (Gimeno et al., 2012; Trenberth et al., 2011). Intense and
55 persistent precipitation events over land cannot be sustained by local terrestrial moisture
56 recycling alone (Brubaker et al., 1993; Dirmeyer et al., 2009; Koster et al., 2004; Trenberth,
57 1999), highlighting ocean-derived moisture as a source of extreme terrestrial precipitation events
58 from.

59 Oceanic evaporation increasingly acts as a source of terrestrial precipitation due to
60 anthropogenic climate change (Gimeno et al., 2020). Rising atmospheric temperatures have led
61 to more rapid evaporation over the oceans than over the land. This climate change response has
62 intensified the oceanic water cycle (Durack et al., 2012), increasing the importance of oceanic
63 evaporation for continental precipitation (Findell et al., 2019). As oceanic moisture evaporates it

64 leaves a signature on sea surface salinity, allowing these fields to be a potential predictor of
65 terrestrial precipitation (Schmitt, 2008).

66 Sea surface salinity has emerged as a potentially useful indicator of evaporation and
67 subsequent moisture export from the ocean (Bengtsson, 2010). A close link exists between the
68 oceanic water cycle and the sea surface salinity anomaly signal: positive anomalies (e.g. saltier
69 waters) indicate evaporation of ocean waters and negative anomalies (e.g. fresher waters)
70 indicate precipitation into the ocean (Durack, 2015). This relationship has led to an investigation
71 into sea surface salinity as a potential seasonal predictor of terrestrial precipitation in the African
72 Sahel (L. Li et al., 2016b), Southwestern U.S. (T. Liu et al., 2018), China (Zeng et al., 2019), and
73 Australia (Rathore et al., 2020). In addition, Li et al. (2016a) and a followup study by Li et al.
74 (2022) showed a strong relationship between springtime sea surface salinity in the northwestern
75 subtropical North Atlantic and summertime precipitation in the U.S. Midwest, revealing sea
76 surface salinity as a skillful *seasonal* predictor of U.S. Midwest summertime rainfall.

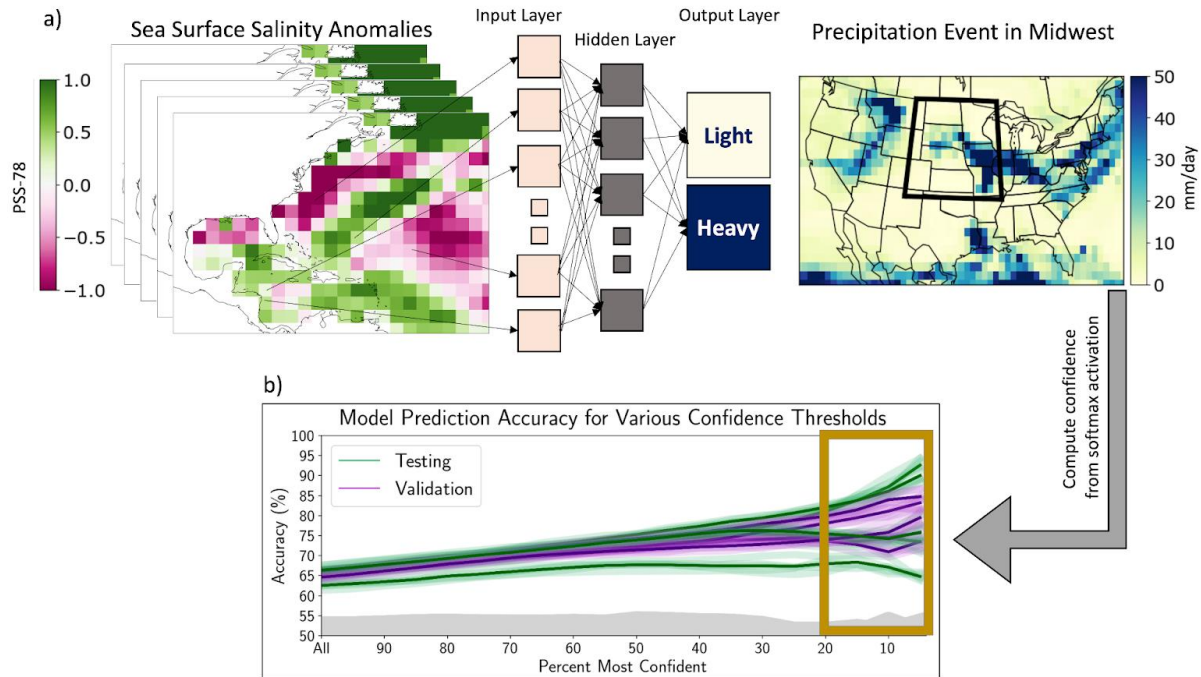
77 Here, we explore the predictability provided by North Atlantic sea surface salinity for
78 *subseasonal* prediction of summertime U.S. Midwest precipitation. Subseasonal prediction (e.g.
79 2 weeks to one season ahead) bridges the gap between weather and climate (Lang et al., 2020)
80 and supports sufficient lead time for storm and flood preparedness and informed resource
81 management (DeFlorio et al., 2021). Heavy Midwest rainfall events in the summertime are
82 particularly challenging to predict (L. Li et al., 2022; Z. Li & O’Gorman, 2020), yet the damage
83 from these events can be extensive (Trenberth & Guillemot, 1996). For example, historic
84 flooding throughout the Midwest region in spring-summer of 2013, dubbed a 500-year flooding
85 event by a U.S. Geological Survey press release, resulted in over 10 fatalities and \$400 million
86 damages. Given the difficult predictive nature of summertime heavy rainfall events, we focus on
87 identifying “forecasts of opportunity”, e.g. predictions with high skill and confidence due to a
88 predictable state of the climate system (Mariotti et al., 2020), and pinpointing their sources of
89 predictability. To connect the climate model analysis to real-world dynamics, we employ a
90 moisture tracking algorithm to determine the North Atlantic sources of evaporation that
91 eventually fall in the Midwest as heavy precipitation events. This study reveals sea surface
92 salinity as an effective subseasonal predictor for forecasts of opportunity of summertime
93 Midwest heavy precipitation events.

94

95 **2 Data and Methods**

96 2.1 Climate Model Data Preprocessing

97 Artificial neural networks are trained to ingest maps of sea surface salinity anomaly maps
98 to classify precipitation events into light or heavy precipitation events over the U.S. Midwest at
99 leads of 0-56 days. Training neural networks requires a large amount of data (Adi et al., 2020),
100 but observed daily sea surface salinity fields are not readily available in a usable (e.g. gridded)
101 format (H. Wang et al., 2022). The few reanalysis datasets that provide daily sea surface salinity
102 fields either do not cover the North Atlantic region needed for this study (e.g. the Global
103 Tropical Moored Buoy Array) or do not have a long enough time series for adequate training
104 (e.g. only ~30 years are provided by the Global Ocean Forecasting System HYCOM, which is
105 insufficient for training in this study). Therefore, we take advantage of the long-running daily,
106 gridded data from the Community Earth System Model Version 2- Large Ensemble (CESM2-
107 LE; Danabasoglu et al., 2020) for analysis of 1,000 years of climate model data.



108
 109 Figure 1. a) Schematic of the neural network architecture used in this study for a 21-day lead. b) The
 110 accuracy vs. confidence for 5 testing (green) and validation (purple) members using 5 random seeds each
 111 (light lines; dark lines represent the average) for 21-day lead predictions. Confidence is computed using
 112 the softmax activation on the output layer of the network in (a). A random network is represented with the
 113 gray shading. The gold box highlights the 20% most confident predictions.

114
 115 We use 1850-1949 historical daily data from 10 CESM2 ensemble members, in which
 116 each ensemble member is considered to be an independent realization of the historical climate
 117 (Rodgers et al., 2021). Sea surface salinity fields in units based on the Practical Salinity Scale
 118 1978 (PSS-78) span May-August to capture the U.S. Midwest summer. Daily anomalies are
 119 computed via subtraction of the linear trend at each grid point of the ensemble mean for each
 120 calendar-day of the year to remove the forced response, then smoothed with a 3-day running
 121 mean. Sea surface salinity anomalies span the North Atlantic region from 8N - 50N, 265E -
 122 320E, including the Gulf of Mexico, but excluding all data from the Pacific (Fig. 1a left).

123 We use raw precipitation fields (e.g. not anomalies) of a 3-day cumulative sum averaged
 124 over the Midwest region- defined as 36N - 49N, 254E - 270E (Fig. 1a right). A Poisson
 125 weighting strategy (Fig. S1) adapted from Ford et al. (2018) is applied to the precipitation time
 126 series to smooth data as lead time increases for a seamless transition across timescales assessed
 127 (Hoskins, 2013). This technique broadens the event window to shift from deterministic to
 128 probabilistic forecasts and account for uncertainty as lead time increases (Fig. S1) (Dirmeyer et
 129 al., 2018; Dirmeyer & Ford, 2020; Ford et al., 2018). Once smoothed, periods above the 80th
 130 percentile of precipitation are classified as heavy events, designated as a 1, and the remaining
 131 80% of the data classified as light events, designated as a 0.

132 2.2 Neural Network Setup

133 The feedforward artificial neural network approach consists of a 3-layer neural network:
 134 the input layer (3-day averaged sea surface salinity anomaly maps), 1 hidden layer, and the

135 output layer (classification of light or heavy precipitation event in the Midwest boxed region).
136 Neural networks are trained separately for each lead time. Additional details on data pre-
137 processing and hyperparameter tuning are found in S1-2 and Tables S1-2.
138

139 2.3 Quantifying Forecasts of Opportunity

140 The final network output layer consists of the two nodes of our binary classification setup
141 (Fig. 1a). The softmax activation function is applied to the final layer, transforming the two
142 outputs to values which sum to 1, representing a probability estimate. This probability is used to
143 select the predicted output in that the value which exceeds 0.5 is selected as the prediction. We
144 leverage this output probability as our network confidence (Arcodia et al., 2023; Mayer &
145 Barnes, 2021, 2022), allowing quantification of the prediction confidence. As confidence
146 increases, accuracy also increases, suggesting that the network identifies intermittent patterns in
147 the input salinity maps that lead it to be more confident in its prediction (Fig. 1b). Hereafter, we
148 define the 20% most confident predictions, which are also found to be the most accurate
149 predictions, as *forecasts of opportunity* (Fig. 1b; gold box).
150

151 2.4 Water Accounting Model

152 We employ the Water Accounting Model 2-layers (WAM2layers, version 3.0.0), a Eulerian
153 moisture-tracking model that can trace the path of water from its origin as evaporation, through
154 the atmosphere as water vapor, and to its eventual fate as precipitation elsewhere (van der Ent et
155 al. 2014; van der Ent et al. 2023). The model uses European Centre for Medium-Range Weather
156 Forecasts v5 (ERA5; Hersbach et al. 2020) climate reanalysis data to verify that the oceanic
157 evaporative moisture source regions identified by the neural networks provide the moisture to
158 Midwest precipitation events in the real world. Additional WAM2layers model details are found
159 in S3.

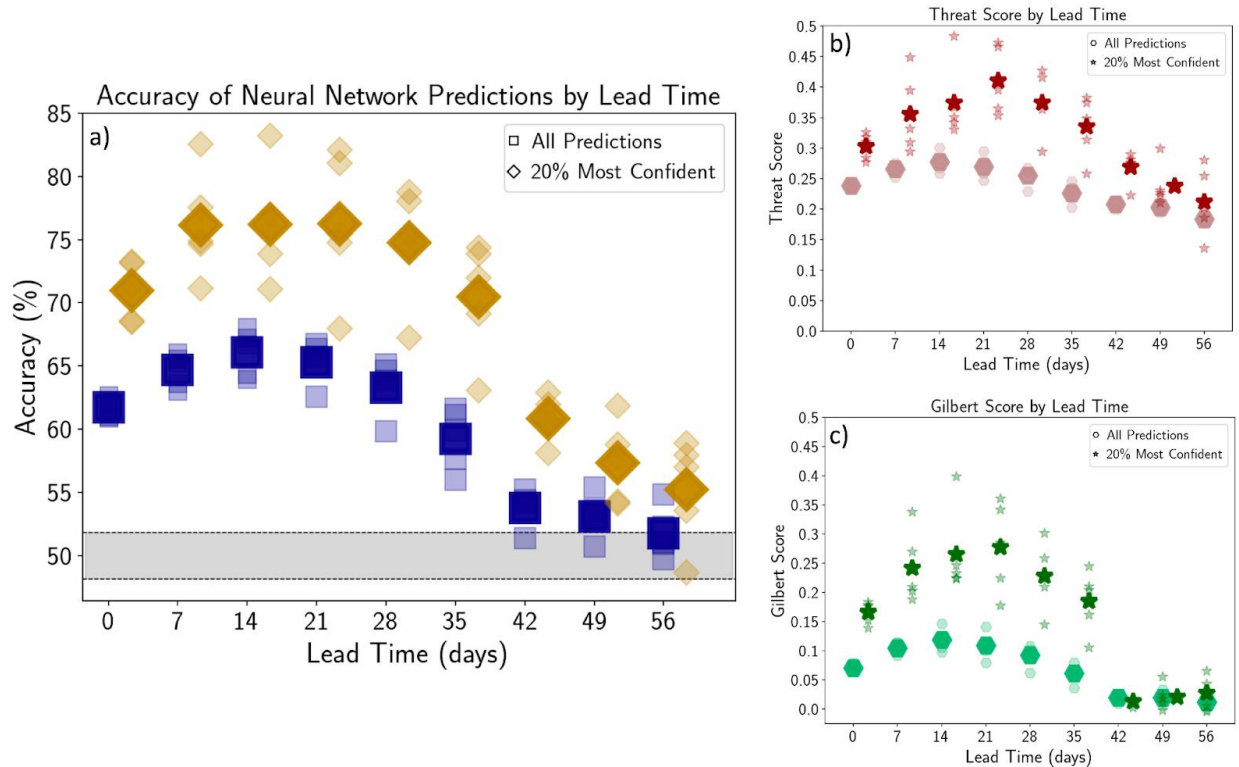
160 3 Results

161 3.1 Subseasonal Forecasts of Opportunity

162 Accuracy for all summertime Midwest precipitation predictions shows the highest skill at
163 leads 14- and 21-days (Fig. 2; blue squares). For the forecasts of opportunity, e.g. the 20% most
164 confident predictions, accuracy peaks at lead 21-days (Fig. 2; gold diamonds), demonstrating
165 that sea surface salinity anomalies serve as a meaningful predictor on subseasonal timescales.
166 Notably, leads 7- through 21-days reveal accuracy above 75% on average for forecasts of
167 opportunity for precipitation event prediction. Skill drops quickly to that of random chance for
168 leads of 35-days and beyond (Fig. 2; gray shading).

169 Fig. 2a shows accuracies for balanced test data (see S1), meaning the likelihood of a
170 heavy precipitation event is 50%. However, based on the definition of a heavy event (>80th
171 percentile), the true likelihood of a heavy event is 20%. We use two skill scores: 1. Threat Score
172 (Fig. 2b) and 2. Gilbert Skill Score (Fig. 2c); see S4 for definitions. These scores are verification
173 metrics of forecasts in which a score of zero denotes no skill, or random chance, and a skill of
174 one is a perfect score. Skill scores are used to evaluate the performance of the networks on
175 unbalanced data to determine if network prediction skill is due to accurate predictions of both
176 classes, or if the network has learned only the majority class. The variation in skill as a function

177 of lead time follows a similar pattern for the balanced and unbalanced datasets, with a peak in
 178 skill at subseasonal lead time of 21 days, particularly for forecasts of opportunity. Networks have
 179 learned patterns within the data to not only predict light but also heavy events, demonstrating the
 180 utility of sea surface salinity as a predictor for high-impact heavy precipitation events.
 181



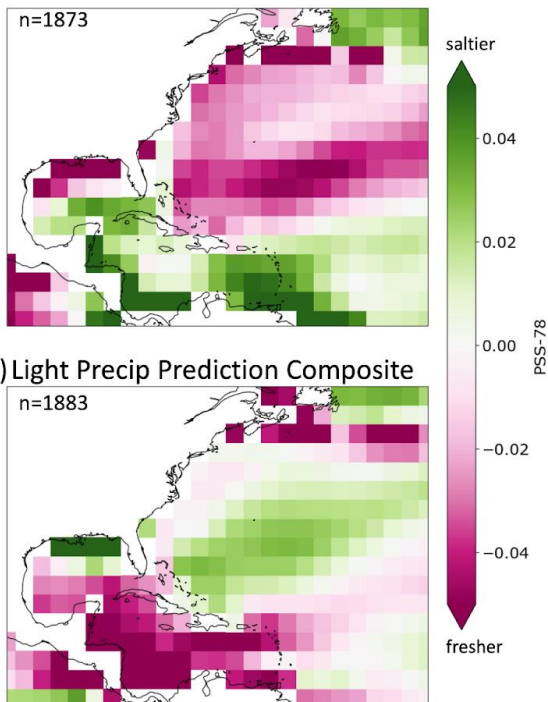
182
 183 Figure 2. a) Accuracy as a function of lead time in days for all predictions (blue squares) and forecasts of
 184 opportunity (gold diamonds). The lightly shaded shapes represent the averaged accuracy from five
 185 random seeds for each test ensemble member with balanced data, and the darker, larger shapes represent
 186 the average accuracy from all 5 test ensemble members. The gray shading denotes the 99% confidence
 187 intervals of a binomial probability (e.g. random chance). b) The Threat Score as a function of lead time
 188 computed on predictions with unbalanced data for all predictions (hexagons) and forecasts of opportunity
 189 (stars). c) Same as b) but for the Gilbert Skill Score. For (b) and (c), a score of zero denotes no skill, or
 190 random chance, and a skill of one is a perfect score.
 191

192 After determining that the networks can result in skillful and confident predictions on
 193 subseasonal lead time times, we want to know *why* the network made these predictions. We find
 194 that for skillful forecasts of opportunity for heavy precipitation, sea surface salinity anomalies in
 195 the Caribbean Sea and Gulf of Mexico are predominantly positive (Fig. 3a). That is, saltier
 196 waters in these regions imply evaporation and atmospheric moisture available for transportation
 197 out of the region. Conversely, for skillful light precipitation predictions, we find negative sea
 198 surface salinity anomalies, indicating precipitation (Fig. 3b). This pattern reflects less
 199 atmospheric moisture from the oceanic source region available to be transported away, resulting
 200 in a confident subseasonal predictions of no heavy rainfall event.

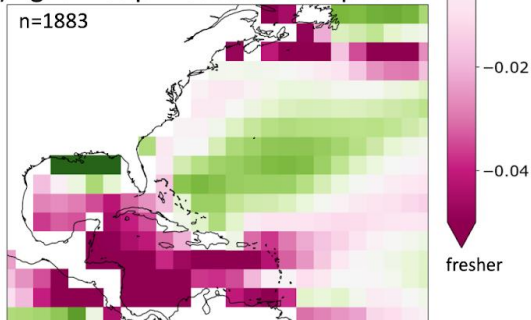
201 We complement the salinity composite maps associated with forecasts of opportunity
 202 with *explainable artificial intelligence* (XAI) to pinpoint regions that the network deems as
 203 important in making its prediction (e.g. Arcodia et al., 2023; Mamalakis, Barnes, et al., 2022;

204 Mayer & Barnes, 2021; McGovern et al., 2019; Pegion et al., 2022; Rader et al., 2022). Here, the
 205 *gradient* method is applied to compute the gradient of the network output with respect to the
 206 input grid points to visualize the sensitivity of the networks to the salinity anomalies at lead 21-
 207 days (Mamalakis, Ebert-Uphoff, et al., 2022) (Fig. 3c; composites and heatmaps for all leads in
 208 Figs. S3 and S4). For correct and confident heavy predictions, the sensitivity of the network to
 209 changes in salinity anomalies is most prominent in the Caribbean Sea and Gulf of Mexico.
 210 Saltier waters in these regions are found to increase confidence in heavy predictions. Regions
 211 with near-zero salinity anomalies south of Jamaica and negative salinity anomalies along the
 212 East Coast in the Gulf Stream region decrease confidence in heavy predictions. That is, network
 213 confidence for heavy subseasonal predictions strengthens as water becomes saltier in the
 214 Caribbean and Gulf of Mexico. Thus, anomalously salty waters in the Caribbean and Gulf of
 215 Mexico provide predictability for heavy precipitation events in the U.S. Midwest on subseasonal
 216 timescales.
 217
 218
 219
 220

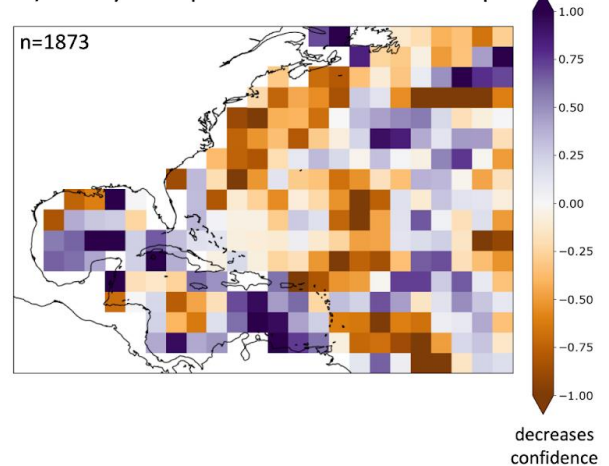
a) Heavy Precip Prediction Composite



b) Light Precip Prediction Composite



c) Heavy Precip Prediction XAI Heatmap



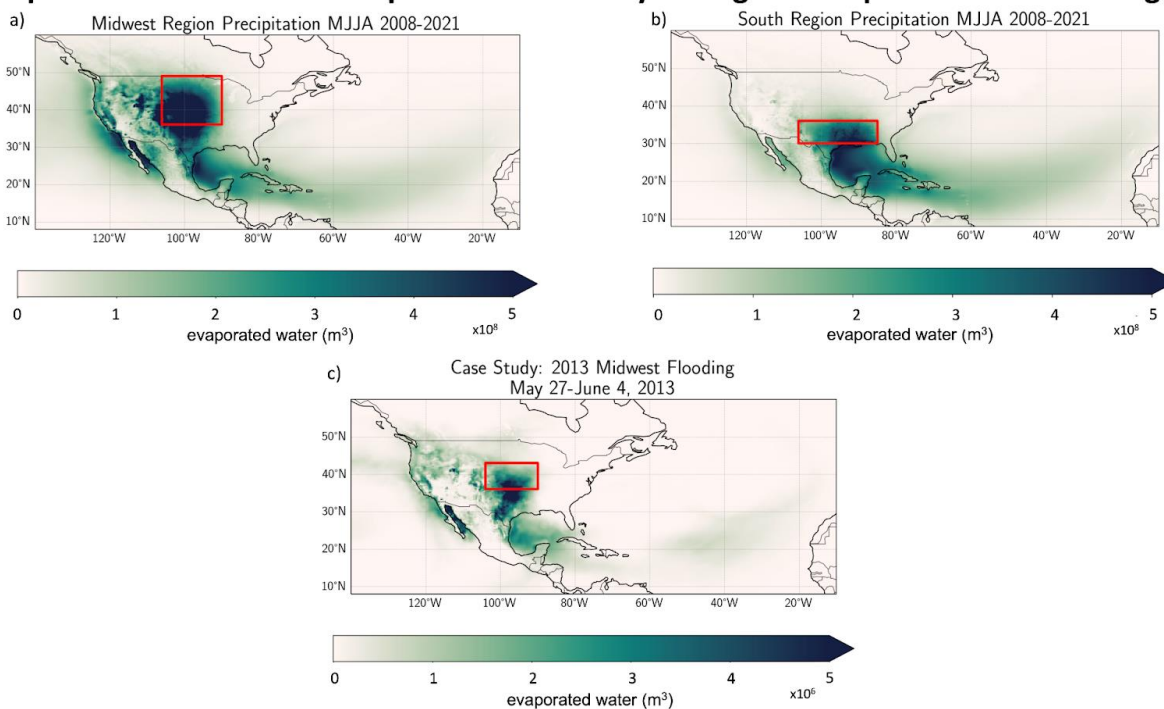
221
 222 Figure 3. a-b) Composite of the sea surface salinity anomalies in PSS-78 for input maps of the 20% most
 223 confident, correct predictions for a 21-day lead for heavy predictions (a) and light predictions (b).
 224 Composites use input from each test ensemble member from the neural network initialized with the
 225 random seed that results in the highest accuracy. c) Saliency XAI composited heatmaps for the same days
 226 as the input maps as (a). The colorbar is a unitless measure of sensitivity. The number n represents the
 227 number of samples per composite.
 228

229 3.2 Moisture Tracking with ERA5

230 The neural networks used thus far were trained, validated, and tested on 1,000 collective
 231 years of CESM2 historical climate model data. Unfortunately, like all climate models, CESM2
 232 exhibits biases which can result in limitations for its use for understanding the real world
 233 (Simpson et al., 2020). Therefore, we employ the WAM2layers model and present-day reanalysis
 234 data (van der Ent et al. 2023) to track where evaporation occurred, which would later fall as
 235 precipitation in a specific region. We track moisture within ERA5 using the WAM2layers model
 236 for May-August (MJJA) from 2008-2021 to pinpoint the origin of all moisture which eventually
 237 falls in the Midwest region (Fig. 4a). The majority of Midwest moisture is found to be locally
 238 recycled, consistent with Bosilovich and Schubert (2002) who showed the largest source of
 239 precipitation in the midwestern U.S. came from local moisture recycling. However, we also find
 240 that summertime Midwest precipitation has an *oceanic* moisture source in the Gulf of Mexico
 241 and the Caribbean Sea regions without recycling, consistent with the regions of sea surface
 242 salinity anomalies identified by the neural networks as relevant for forecasts of opportunity (Fig.
 243 3).

244 Another primary moisture source region for the Midwest is the area directly to the south
 245 (Fig. 4a), indicating that the southern U.S. acts as an additional moisture source region. The
 246 WAM2layers results for moisture-tracking of the southern U.S. also highlight the Gulf of
 247 Mexico and Caribbean Sea (Fig. 4b). Moisture which evaporates over the Gulf of Mexico and
 248 Caribbean Sea likely acts as a moisture source for Midwest precipitation in 2 ways: 1) moisture
 249 is directly transported and precipitates in the Midwest, or 2) moisture falls as precipitation in the
 250 southern U.S. region which is then locally recycled and transported north to eventually
 251 precipitate in the Midwest. Thus, the networks have identified physically meaningful sources of
 252 predictability, consistent with the patterns found in the composite and XAI maps (Fig. 3), which
 253 can ultimately provide subseasonal prediction skill for U.S. Midwest heavy rainfall events.
 254

Evaporation Sources for Precipitation Eventually Falling as Precipitation in Boxed Region



256 Figure 4. The sum of the evaporated water (in cubic meters) which fell as precipitation in the red boxed
257 regions computed using the WAM2layers backtracking algorithm for the Midwest (a) and South U.S.
258 region (b) for May-August from 2008-2021. c) shows the same, but for the southern Midwest region (red
259 box) for May 27-June 4, 2013.

260

261 Lastly, we analyze a case study to verify the Gulf of Mexico and Caribbean Sea can
262 provide moisture sources for specific heavy precipitation events in the Midwest. We analyze a 9-
263 day period of intense rainfall in the Midwest region from May 27 - June 4, 2013 when over 150
264 mm of rainfall was recorded in the Missouri and southeastern Midwest areas (USGS, 2013) (Fig.
265 4c). We find that the local region (red box), southern U.S., and Gulf of Mexico/ Caribbean Sea
266 are the largest moisture source regions for the observed extreme precipitation. Approximately
267 22% of the moisture originated from the Caribbean Sea and Gulf of Mexico region and was
268 directly transported and precipitated in the Midwest during this event (see S5 and Fig. S4), while
269 only 11% of the moisture was locally recycled. An additional case study is shown in
270 Supplemental Fig. 5 for the 2011 Missouri River Flooding events from May-June in which
271 approximately 21% directly originated from the Caribbean and Gulf of Mexico region and 14%
272 of the moisture was locally recycled.

273 The results from the WAM2layers water tracking model reveal that evaporation over the
274 Gulf of Mexico and Caribbean Sea acts as a moisture source for precipitation over the Midwest
275 in summertime. These results support our findings that evaporation in these regions indicated by
276 sea surface salinity anomalies can provide predictive skill for heavy summertime Midwest
277 precipitation events.

278 **4 Discussion**

279 This analysis has revealed that salty waters indicative of evaporation in the Caribbean
280 and Gulf of Mexico (Fig. 3) provide predictability for subseasonal forecasts of opportunity for
281 heavy Midwest precipitation events (Fig. 2). We discuss a potential physical link for how the
282 evaporative moisture source regions, identified by neural networks, provide moisture that
283 ultimately precipitates in the Midwest region. The Caribbean Sea has been documented to
284 provide significant moisture sources for Midwest extreme precipitation events via dynamical
285 links from low-level jets (Dirmeyer & Kinter, 2010). In the summertime, a branch of the
286 Caribbean Low-level Jet (CLLJ) turns northward and connects with the Great Plain Low-level
287 Jet (GPLLJ) (Amador, 1998; Cook & Vizy, 2010). This causes a shift in westward moisture
288 transport over the Caribbean Sea to northward transport over the continental U.S. into the Great
289 Plains and Midwest regions (C. Wang et al., 2007). The interactions of these jets are intimately
290 tied to the North Atlantic Subtropical High (NASH), a robust atmospheric high pressure in the
291 North Atlantic region which impacts the strength and location of the low-level jets and their
292 surface evaporation (C. Wang et al., 2007). The lower branch of the NASH is reflected in the
293 swooping evaporated water feature found from the WAM2layers analysis in Fig. 4, supporting
294 the dynamical link between subtropical jet features and Midwest precipitation. Putting it all
295 together, evaporation in the Caribbean and Gulf of Mexico increases atmospheric moisture
296 availability which is then transported westward by the Caribbean Low-level Jet and northward
297 into continental U.S. and Midwest by the Great Plains Low-level jet.

298 Li et al. (2018) showed that a soil moisture feedback mechanism connects North Atlantic
299 sea surface salinity anomalies to Midwest summertime precipitation. Enhanced moisture export
300 from the subtropical North Atlantic contributes to extreme rainfall in the southern U.S. leading to

301 increased soil moisture. This soil moisture feedback causes enhanced evaporation and
302 atmospheric convection, which intensifies the GPLLJ and transports moisture to the Midwest
303 region. Additional research into the prediction of the location and intensity of these jets and the
304 NASH (e.g. Ferguson, 2022; García-Martínez & Bolasina, 2020; Krishnamurthy et al., 2015;
305 Malloy & Kirtman, 2020) could provide added predictive skill for forecasts of opportunity for
306 Midwest precipitation events.

307 Sea surface salinity biases have been documented in CESM2 linked to precipitation
308 biases (Simpson et al., 2020; Wei et al., 2021) with a slightly fresh overall salinity bias (Y. Liu et
309 al., 2022). There are also discrepancies between satellite and in-situ sea surface salinity data due
310 to both observational and sampling errors which provide constraints for ocean models
311 (Vinogradova et al., 2019). Further, CESM2 sea surface salinity data is taken as the average of
312 the upper 10m of the ocean. Boutin et al. (2016) show that near-surface stratification of salinity
313 exists in the upper 1m and subseasonal prediction could vary based on this upper ocean
314 resolution (Subramanian et al., 2019). We note that the predictive skill of heavy precipitation
315 events using higher vertical resolution sea surface salinity data may vary as this could more
316 effectively capture skin-layer evaporation intensity, rather than muted anomalies represented in
317 the 0-10m volume average, but we leave this investigation for future work.

318 **5 Conclusions**

319 This study is the first peer-reviewed documentation to demonstrate the utility of North
320 Atlantic sea surface salinity anomalies as a skillful subseasonal predictor of heavy Midwest
321 summertime precipitation events. We employ a machine learning approach using neural
322 networks to quantify the subseasonal predictability of heavy summertime rainfall events in the
323 U.S. Midwest region using 3-day North Atlantic sea surface salinity fields. Using a statistical
324 smoothing for a seamless transition across timescales, we assess predictability for lead times
325 from 0-days to 56-days. We find that predictive skill is highest on subseasonal timescales with a
326 peak at 21-day lead, particularly for forecasts of opportunity, e.g. predictions which are both
327 confident and accurate. Output from neural networks allows us to identify predictions which
328 result in forecasts of opportunity. Using explainable artificial intelligence, we create heatmaps of
329 the most sensitive regions of salinity anomalies in the tropical and North Atlantic which provide
330 skill for forecasts of opportunity. Positive sea surface salinity anomalies (which indicate
331 evaporation and increased atmospheric moisture availability) in the Caribbean and Gulf of
332 Mexico provide predictability for the forecasts of opportunity for heavy precipitation events.
333 Consistent with previous research highlighting subtropical North Atlantic moisture as a source of
334 U.S. terrestrial precipitation (Gimeno et al., 2010; L. Li et al., 2016a, 2022; van der Ent et al.,
335 2010), our results support a physically consistent link between evaporation in the Caribbean and
336 Gulf of Mexico and heavy precipitation in the Midwest via low-level jets. Output from the
337 WAM2layers moisture-tracking model reveals that the regions of evaporation identified by
338 neural networks within CESM2 simulations provide moisture to the Midwest region in the ERA5
339 atmospheric reanalysis. The Caribbean Sea and Gulf of Mexico are found to provide a direct
340 oceanic moisture source for Midwest precipitation, in part without moisture recycling, linking
341 the salinity anomalies to subseasonal predictive skill of Midwest precipitation. These results
342 complement the explainable artificial intelligence findings to reveal robust and physically
343 meaningful sources of summertime heavy Midwest precipitation predictability via Atlantic sea
344 surface salinity anomalies.

345 **Acknowledgments**

346 This study was performed as part of the Program for Climate Model Diagnosis and
347 Intercomparison (PCMDI), supported by the Regional and Global Modeling Analysis (RGMA)
348 program area of U.S. DOE's Biological and Environmental Research (BER) Program. Work was
349 performed under the auspices of the U.S. DOE by Lawrence Livermore National Laboratory
350 under contract DEAC52-07NA27344. LLNL Release Number: LLNL-JNRL-859091. The
351 authors declare no conflict of interest.

352

353 **Open Research**

354 CESM2 Large Ensemble Data are available freely to the public at
355 www.cesm.ucar.edu/community-projects/lens2. The code for the Water Accounting Model 2-
356 layers is available on GitHub, and is posted to the Zenodo permanent repository:
357 <https://doi.org/10.5281/zenodo.8172344>. The ERA5 data were downloaded from the Copernicus
358 Climate Data Store, and are freely available at
359 <https://cds.climate.copernicus.eu/cdsapp#!/dataset/reanalysis-era5-complete?tab=overview>.
360 All Python code for processing data and figures for this analysis will be available to the public
361 on Github and converted to a permanent repository on Zenodo at the time of acceptance for
362 publication.

363

364 **References**

- 365 Adi, E., Anwar, A., Baig, Z., & Zeadally, S. (2020). Machine learning and data analytics for the IoT.
366 *Neural Computing & Applications*, 32(20), 16205–16233.
- 367 Adler, R. F., Huffman, G. J., Chang, A., Ferraro, R., Xie, P.-P., Janowiak, J., Rudolf, B., Schneider, U.,
368 Curtis, S., Bolvin, D., Gruber, A., Susskind, J., Arkin, P., & Nelkin, E. (2003). The Version-2 Global
369 Precipitation Climatology Project (GPCP) Monthly Precipitation Analysis (1979–Present). *Journal*
370 *of Hydrometeorology*, 4(6), 1147–1167.
- 371 Amador, J. A. (1998). A climate feature of the tropical Americas: The trade wind easterly jet. *Topicos*
372 *Meteorologicos Oceanograficos*.
- 373 Arcodia, M. C., Barnes, E. A., Mayer, K. J., Lee, J., Ordonez, A., & Ahn, M.-S. (2023). Assessing
374 decadal variability of subseasonal forecasts of opportunity using explainable AI. *Environmental*
375 *Research: Climate*, 2(4), 045002.
- 376 Bengtsson, L. (2010). The global atmospheric water cycle. *Environmental Research Letters*, 5(2),

- 377 025202.
- 378 Bosilovich, M. G., & Schubert, S. D. (2002). Water Vapor Tracers as Diagnostics of the Regional
 379 Hydrologic Cycle. *Journal of Hydrometeorology*, 3(2), 149–165.
- 380 Boutin, J., Chao, Y., Asher, W. E., Delcroix, T., Drucker, R., Drushka, K., Kolodziejczyk, N., Lee, T.,
 381 Reul, N., Reverdin, G., Schanze, J., Soloviev, A., Yu, L., Anderson, J., Brucker, L., Dinnat, E.,
 382 Santos-Garcia, A., Jones, W. L., Maes, C., ... Ward, B. (2016). Satellite and In Situ Salinity:
 383 Understanding Near-Surface Stratification and Subfootprint Variability. *Bulletin of the American*
 384 *Meteorological Society*, 97(8), 1391–1407.
- 385 Brubaker, K. L., Entekhabi, D., & Eagleson, P. S. (1993). Estimation of Continental Precipitation
 386 Recycling. *Journal of Climate*, 6(6), 1077–1089.
- 387 Cook, K. H., & Vizy, E. K. (2010). Hydrodynamics of the Caribbean Low-Level Jet and Its Relationship
 388 to Precipitation. *Journal of Climate*, 23(6), 1477–1494.
- 389 Danabasoglu, G., Lamarque, J.-F., Bacmeister, J., Bailey, D. A., DuVivier, A. K., Edwards, J., Emmons,
 390 L. K., Fasullo, J., Garcia, R., Gettelman, A., Hannay, C., Holland, M. M., Large, W. G., Lauritzen,
 391 P. H., Lawrence, D. M., Lenaerts, J. T. M., Lindsay, K., Lipscomb, W. H., Mills, M. J., ... Strand,
 392 W. G. (2020). The community earth system model version 2 (CESM2). *Journal of Advances in*
 393 *Modeling Earth Systems*, 12(2). <https://doi.org/10.1029/2019ms001916>
- 394 DeFlorio, M. J., Ralph, F. M., Waliser, D. E., Jones, J., & Anderson, M. L. (2021). *Better Subseasonal-to-*
 395 *Seasonal Forecasts for Water Management*. *Eos*, 102. <https://doi.org/10.1029/2021EO159749>
- 396 Dirmeyer, P. A., Adam Schlosser, C., & Brubaker, K. L. (2009). Precipitation, Recycling, and Land
 397 Memory: An Integrated Analysis. *Journal of Hydrometeorology*, 10(1), 278–288.
- 398 Dirmeyer, P. A., & Ford, T. W. (2020). A Technique for Seamless Forecast Construction and Validation
 399 from Weather to Monthly Time Scales. *Monthly Weather Review*, 148(9), 3589–3603.
- 400 Dirmeyer, P. A., Halder, S., & Bombardi, R. (2018). On the harvest of predictability from land states in a
 401 global forecast model. *Journal of Geophysical Research*, 123(23), 13,111–113,127.
- 402 Dirmeyer, P. A., & Kinter, J. L. (2010). Floods over the U.S. Midwest: A Regional Water Cycle

- 403 Perspective. *Journal of Hydrometeorology*, 11(5), 1172–1181.
- 404 Durack, P. J. (2015). Ocean Salinity and the Global Water Cycle. *Oceanography*, 28(1), 20–31.
- 405 Durack, P. J., Wijffels, S. E., & Matear, R. J. (2012). Ocean salinities reveal strong global water cycle
406 intensification during 1950 to 2000. *Science*, 336(6080), 455–458.
- 407 Ferguson, C. R. (2022). Changes in great plains low-level jet structure and associated precipitation over
408 the 20th century. *Journal of Geophysical Research*, 127(3). <https://doi.org/10.1029/2021jd035859>
- 409 Findell, K. L., Keys, P. W., van der Ent, R. J., Lintner, B. R., Berg, A., & Krasting, J. P. (2019). Rising
410 Temperatures Increase Importance of Oceanic Evaporation as a Source for Continental Precipitation.
411 *Journal of Climate*, 32(22), 7713–7726.
- 412 Ford, T. W., Dirmeyer, P. A., & Benson, D. O. (2018). Evaluation of heat wave forecasts seamlessly
413 across subseasonal timescales. *Npj Climate and Atmospheric Science*, 1(1), 1–9.
- 414 García-Martínez, I. M., & Bollasina, M. A. (2020). Sub-monthly evolution of the Caribbean Low-Level
415 Jet and its relationship with regional precipitation and atmospheric circulation. *Climate Dynamics*,
416 54(9), 4423–4440.
- 417 Gimeno, L., Drumond, A., Nieto, R., Trigo, R. M., & Stohl, A. (2010). On the origin of continental
418 precipitation. *Geophysical Research Letters*, 37(13). <https://doi.org/10.1029/2010gl043712>
- 419 Gimeno, L., Nieto, R., & Sorí, R. (2020). The growing importance of oceanic moisture sources for
420 continental precipitation. *Npj Climate and Atmospheric Science*, 3(1), 1–9.
- 421 Gimeno, L., Stohl, A., Trigo, R. M., Dominguez, F., Yoshimura, K., Yu, L., Drumond, A., Durán-
422 Quesada, A. M., & Nieto, R. (2012). Oceanic and terrestrial sources of continental precipitation.
423 *Reviews of Geophysics*, 50(4). <https://doi.org/10.1029/2012RG000389>
- 424 Hersbach, H., Bell, B., Berrisford, P., Hirahara, S., Horányi, A., Muñoz-Sabater, J., Nicolas, J., Peubey,
425 C., Radu, R., Schepers, D., Simmons, A., Soci, C., Abdalla, S., Abellan, X., Balsamo, G., Bechtold,
426 P., Biavati, G., Bidlot, J., Bonavita, M., ... Jean-Noël Thépaut. (2020). The ERA5 global reanalysis.
427 *Quarterly Journal of the Royal Meteorological Society*, 146(730), 1999–2049.
- 428 Hoskins, B. (2013). The potential for skill across the range of the seamless weather-climate prediction

- 429 problem: a stimulus for our science. *Quarterly Journal of the Royal Meteorological Society*,
430 139(672), 573–584.
- 431 Koster, R. D., Dirmeyer, P. A., Guo, Z., Bonan, G., Chan, E., Cox, P., Gordon, C. T., Kanae, S.,
432 Kowalczyk, E., Lawrence, D., Liu, P., Lu, C.-H., Malyshev, S., McAvaney, B., Mitchell, K., Mocko,
433 D., Oki, T., Oleson, K., Pitman, A., ... GLACE Team. (2004). Regions of strong coupling between
434 soil moisture and precipitation. *Science*, 305(5687), 1138–1140.
- 435 Krishnamurthy, L., Vecchi, G. A., Msadek, R., Wittenberg, A., Delworth, T. L., & Zeng, F. (2015). The
436 Seasonality of the Great Plains Low-Level Jet and ENSO Relationship. *Journal of Climate*, 28(11),
437 4525–4544.
- 438 Lang, A. L., Kathleen, Pegion, & Barnes, E. (2020). Introduction to special collection: “bridging weather
439 and climate: Subseasonal-to-seasonal (S2S) prediction.” *Journal of Geophysical Research*, 125(4).
440 <https://doi.org/10.1029/2019jd031833>
- 441 Li, L., Schmitt, R. W., & Ummenhofer, C. C. (2018). The role of the subtropical North Atlantic water
442 cycle in recent US extreme precipitation events. *Climate Dynamics*, 50(3), 1291–1305.
- 443 Li, L., Schmitt, R. W., & Ummenhofer, C. C. (2022). Skillful long-lead prediction of summertime heavy
444 rainfall in the US Midwest from sea surface salinity. *Geophysical Research Letters*, 49(13).
445 <https://doi.org/10.1029/2022gl098554>
- 446 Li, L., Schmitt, R. W., Ummenhofer, C. C., & Karnauskas, K. B. (2016a). Implications of North Atlantic
447 Sea Surface Salinity for Summer Precipitation over the U.S. Midwest: Mechanisms and Predictive
448 Value. *Journal of Climate*, 29(9), 3143–3159.
- 449 Li, L., Schmitt, R. W., Ummenhofer, C. C., & Karnauskas, K. B. (2016b). North Atlantic salinity as a
450 predictor of Sahel rainfall. *Science Advances*, 2(5), e1501588.
- 451 Liu, T., Schmitt, R. W., & Li, L. (2018). Global Search for Autumn-Lead Sea Surface Salinity Predictors
452 of Winter Precipitation in Southwestern United States. *Geophysical Research Letters*, 45(16), 8445–
453 8454.
- 454 Liu, Y., Cheng, L., Pan, Y., Tan, Z., Abraham, J., Zhang, B., Zhu, J., & Song, J. (2022). How Well Do

- 455 CMIP6 and CMIP5 Models Simulate the Climatological Seasonal Variations in Ocean Salinity?
456 *Advances in Atmospheric Sciences*, 39(10), 1650–1672.
- 457 Li, Z., & O’Gorman, P. A. (2020). Response of Vertical Velocities in Extratropical Precipitation
458 Extremes to Climate Change. *Journal of Climate*, 33(16), 7125–7139.
- 459 Malloy, K. M., & Kirtman, B. P. (2020). Predictability of Midsummer Great Plains Low-Level Jet and
460 Associated Precipitation. *Weather and Forecasting*, 35(1), 215–235.
- 461 Mamalakis, A., Barnes, E. A., & Ebert-Uphoff, I. (2022). Investigating the Fidelity of Explainable
462 Artificial Intelligence Methods for Applications of Convolutional Neural Networks in Geoscience.
463 *Artificial Intelligence for the Earth Systems*, 1(4). <https://doi.org/10.1175/AIES-D-22-0012.1>
- 464 Mamalakis, A., Ebert-Uphoff, I., & Barnes, E. A. (2022). Neural network attribution methods for
465 problems in geoscience: A novel synthetic benchmark dataset. *Environmental Data Science*, 1, e8.
- 466 Mariotti, A., Baggett, C., Barnes, E. A., Becker, E., Butler, A., Collins, D. C., Dirmeyer, P. A., Ferranti,
467 L., Johnson, N. C., Jones, J., Kirtman, B. P., Lang, A. L., Molod, A., Newman, M., Robertson, A.
468 W., Schubert, S., Waliser, D. E., & Albers, J. (2020). Windows of Opportunity for Skillful Forecasts
469 Subseasonal to Seasonal and Beyond. *Bulletin of the American Meteorological Society*, 101(5),
470 E608–E625.
- 471 Mayer, K. J., & Barnes, E. A. (2021). Subseasonal forecasts of opportunity identified by an explainable
472 neural network. *Geophysical Research Letters*, 48(10). <https://doi.org/10.1029/2020gl092092>
- 473 Mayer, K. J., & Barnes, E. A. (2022). Quantifying the effect of climate change on midlatitude subseasonal
474 prediction skill provided by the tropics. *Geophysical Research Letters*, 49(14).
475 <https://doi.org/10.1029/2022gl098663>
- 476 McGovern, A., Lagerquist, R., Gagne, D. J., Eli Jergensen, G., Elmore, K. L., Homeyer, C. R., & Smith,
477 T. (2019). Making the Black Box More Transparent: Understanding the Physical Implications of
478 Machine Learning. *Bulletin of the American Meteorological Society*, 100(11), 2175–2199.
- 479 O’Malley, T., Bursztein, E., Long, J., Chollet, F., Jin, H., Invernizzi, L., & Others. (2019). *KerasTuner*.
480 <https://github.com/keras-team/keras-tuner>

- 481 Pegion, K., Becker, E. J., & Kirtman, B. P. (2022). Understanding Predictability of Daily Southeast U.S.
482 Precipitation Using Explainable Machine Learning. *Artificial Intelligence for the Earth Systems*,
483 *1*(4). <https://doi.org/10.1175/AIES-D-22-0011.1>
- 484 Rader, J. K., Barnes, E. A., Ebert-Uphoff, I., & Anderson, C. (2022). Detection of forced change within
485 combined climate fields using explainable neural networks. *Journal of Advances in Modeling Earth*
486 *Systems*, *14*(7). <https://doi.org/10.1029/2021ms002941>
- 487 Rathore, S., Bindoff, N. L., Ummenhofer, C. C., Phillips, H. E., & Feng, M. (2020). Near-Surface Salinity
488 Reveals the Oceanic Sources of Moisture for Australian Precipitation through Atmospheric Moisture
489 Transport. *Journal of Climate*, *33*(15), 6707–6730.
- 490 Rodgers, K. B., Lee, S.-S., Rosenbloom, N., Timmermann, A., Danabasoglu, G., Deser, C., Edwards, J.,
491 Kim, J.-E., Simpson, I. R., Stein, K., Stuecker, M. F., Yamaguchi, R., Bódai, T., Chung, E.-S.,
492 Huang, L., Kim, W. M., Lamarque, J.-F., Lombardozzi, D. L., Wieder, W. R., & Yeager, S. G.
493 (2021). Ubiquity of human-induced changes in climate variability. *Earth System Dynamics*, *12*(4),
494 1393–1411.
- 495 Schmitt, R. (2008). Salinity and the global water cycle. *Oceanography*, *21*, 12–19.
- 496 Simpson, I. R., Bacmeister, J., Neale, R. B., Hannay, C., Gettelman, A., Garcia, R. R., Lauritzen, P. H.,
497 Marsh, D. R., Mills, M. J., Medeiros, B., & Richter, J. H. (2020). An evaluation of the large-scale
498 atmospheric circulation and its variability in CESM2 and other CMIP models. *Journal of*
499 *Geophysical Research*, *125*(13). <https://doi.org/10.1029/2020jd032835>
- 500 Subramanian, A. C., Balmaseda, M. A., Centurioni, L., Chattopadhyay, R., Cornuelle, B. D., DeMott, C.,
501 Flatau, M., Fujii, Y., Giglio, D., Gille, S. T., Hamill, T. M., Hendon, H., Hoteit, I., Kumar, A., Lee,
502 J.-H., Lucas, A. J., Mahadevan, A., Matsueda, M., Nam, S., ... Zhang, C. (2019). Ocean
503 Observations to Improve Our Understanding, Modeling, and Forecasting of Subseasonal-to-Seasonal
504 Variability. *Frontiers in Marine Science*, *6*. <https://doi.org/10.3389/fmars.2019.00427>
- 505 Trenberth, K. E. (1999). Atmospheric Moisture Recycling: Role of Advection and Local Evaporation.
506 *Journal of Climate*, *12*(5), 1368–1381.

- 507 Trenberth, K. E., Fasullo, J. T., & Mackaro, J. (2011). Atmospheric Moisture Transports from Ocean to
508 Land and Global Energy Flows in Reanalyses. *Journal of Climate*, 24(18), 4907–4924.
- 509 Trenberth, K. E., & Guillemot, C. J. (1996). Physical Processes Involved in the 1988 Drought and 1993
510 Floods in North America. *Journal of Climate*, 9(6), 1288–1298.
- 511 Trenberth, K. E., Smith, L., Qian, T., Dai, A., & Fasullo, J. (2007). Estimates of the Global Water Budget
512 and Its Annual Cycle Using Observational and Model Data. *Journal of Hydrometeorology*, 8(4),
513 758–769.
- 514 U.S. Geological Survey Office. (2013, June 3). *Friday Storms Caused Record Flooding on Fourche*
515 *LaFave River in Scott and Yell Counties - U.S. Geological Survey Press release*. LegiStorm.
516 [https://www.legistorm.com/stormfeed/view_rss/278658/organization/35286/title/friday-storms-](https://www.legistorm.com/stormfeed/view_rss/278658/organization/35286/title/friday-storms-caused-record-flooding-on-fourche-lafave-river-in-scott-and-yell-counties.html)
517 [caused-record-flooding-on-fourche-lafave-river-in-scott-and-yell-counties.html](https://www.legistorm.com/stormfeed/view_rss/278658/organization/35286/title/friday-storms-caused-record-flooding-on-fourche-lafave-river-in-scott-and-yell-counties.html)
- 518 USGS. (2013). *May-June 2013 Midwest Floods*. [https://www.usgs.gov/mission-areas/water-](https://www.usgs.gov/mission-areas/water-resources/science/may-june-2013-midwest-floods)
519 [resources/science/may-june-2013-midwest-floods](https://www.usgs.gov/mission-areas/water-resources/science/may-june-2013-midwest-floods)
- 520 van der Ent, R. J., Savenije, H. H. G., Schaeffli, B., & Steele-Dunne, S. C. (2010). Origin and fate of
521 atmospheric moisture over continents. *Water Resources Research*, 46(9).
522 <https://doi.org/10.1029/2010wr009127>
- 523 Vinogradova, N., Lee, T., Boutin, J., Drushka, K., Fournier, S., Sabia, R., Stammer, D., Bayler, E., Reul,
524 N., Gordon, A., Melnichenko, O., Li, L., Hackert, E., Martin, M., Kolodziejczyk, N., Hasson, A.,
525 Brown, S., Misra, S., & Lindstrom, E. (2019). Satellite Salinity Observing System: Recent
526 Discoveries and the Way Forward. *Frontiers in Marine Science*, 6.
527 <https://doi.org/10.3389/fmars.2019.00243>
- 528 Wang, C., Lee, S.-K., & Enfield, D. B. (2007). Impact of the Atlantic Warm Pool on the Summer Climate
529 of the Western Hemisphere. *Journal of Climate*, 20(20), 5021–5040.
- 530 Wang, H., You, Z., Guo, H., Zhang, W., Xu, P., & Ren, K. (2022). Quality Assessment of Sea Surface
531 Salinity from Multiple Ocean Reanalysis Products. *Journal of Marine Science and Engineering*,
532 11(1), 54.

533 Wei, H.-H., Subramanian, A. C., Karlsrukas, K. B., DeMott, C. A., Mazloff, M. R., & Balmaseda, M. A.

534 (2021). Tropical pacific air-sea interaction processes and biases in CESM2 and their relation to El

535 Niño development. *Journal of Geophysical Research, C: Oceans*, 126(6).

536 <https://doi.org/10.1029/2020jc016967>

537 Zeng, L., Schmitt, R. W., Li, L., Wang, Q., & Wang, D. (2019). Forecast of summer precipitation in the

538 Yangtze River Valley based on South China Sea springtime sea surface salinity. *Climate Dynamics*,

539 53(9), 5495–5509.

540

541 **References from Supporting Information**

542 O'Malley, T., Bursztein, E., Long, J., Chollet, F., Jin, H., Invernizzi, L., & Others. (2019). *KerasTuner*.

543 <https://github.com/keras-team/keras-tuner>

544 Prusa, J., Khoshgoftaar, T. M., Dittman, D. J., & Napolitano, A. (2015). Using Random Undersampling to

545 Alleviate Class Imbalance on Tweet Sentiment Data. *2015 IEEE International Conference on*

546 *Information Reuse and Integration*, 197–202.

547